



HAL
open science

$^{240}\text{Pu}/^{239}\text{Pu}$ signatures allow refining the chronology of radionuclide fallout in South America

Pierre-Alexis Chaboche, Fabien Pointurier, Pierre Sabatier, Anthony Foucher, Tales Tiecher, Jean P. G. Minella, Marcos Tassano, Amélie Hubert, Sergio Morera, Stéphane Guédron, et al.

► To cite this version:

Pierre-Alexis Chaboche, Fabien Pointurier, Pierre Sabatier, Anthony Foucher, Tales Tiecher, et al.. $^{240}\text{Pu}/^{239}\text{Pu}$ signatures allow refining the chronology of radionuclide fallout in South America. Science of the Total Environment, 2022, 843, pp.156943. 10.1016/j.scitotenv.2022.156943 . cea-03712024

HAL Id: cea-03712024

<https://cea.hal.science/cea-03712024>

Submitted on 2 Jul 2022

HAL is a multi-disciplinary open access archive for the deposit and dissemination of scientific research documents, whether they are published or not. The documents may come from teaching and research institutions in France or abroad, or from public or private research centers.

L'archive ouverte pluridisciplinaire **HAL**, est destinée au dépôt et à la diffusion de documents scientifiques de niveau recherche, publiés ou non, émanant des établissements d'enseignement et de recherche français ou étrangers, des laboratoires publics ou privés.



Distributed under a Creative Commons Attribution - NonCommercial - NoDerivatives 4.0 International License

Title

$^{240}\text{Pu}/^{239}\text{Pu}$ signatures allow refining the chronology of radionuclide fallout in South America.

Authors

Pierre-Alexis Chaboche^{1*}, Fabien Pointurier², Pierre Sabatier³, Anthony Foucher¹, Tales Tiecher⁴, Jean P.G. Minella⁵, Marcos Tassano⁶, Amélie Hubert², Sergio Morera⁷, Stéphane Guédron⁸, Christophe Ardois⁹, Béatrice Boulet⁹, Catherine Cossonnet^{†9}, Pablo Cabral⁶, Mirel Cabrera⁶, Guillermo Chalar¹⁰, Olivier Evrard^{1*}

Affiliations

¹Laboratoire des Sciences du Climat et de l'Environnement (LSCE/IPSL), Unité Mixte de Recherche 8212 (CEA-CNRS-UVSQ), Université Paris-Saclay, Gif-sur-Yvette, France.

²CEA, DAM, DIF, F-91297 Arpajon, France.

³EDYTEM, Université Savoie-Mont Blanc, CNRS, 73370, Le Bourget du Lac, France.

⁴Department of Soil Science, Federal University of Rio Grande do Sul, Bento Gonçalves Ave. 7712, 91540-000 Porto Alegre, RS, Brazil.

⁵Department of Soils, Federal University of Santa Maria, 97105-900 Santa Maria, Brazil.

⁶Laboratorio de Radioquímica, Centro de Investigaciones Nucleares, Facultad de Ciencias, Universidad de la República, Montevideo, Uruguay.

⁷Instituto Geofísico del Perú, Universidad Nacional Agraria La Molina, 15081 Lima, Peru.

⁸Univ. Grenoble Alpes, Univ. Savoie Mont Blanc, CNRS, IRD, IFSTTAR, ISTERre, 38000 Grenoble, France.

⁹Institut de Radioprotection et de Sûreté nucléaire, Bât 501, bois des Rames, 91400, Orsay, France.

¹⁰Sección Limnología, Facultad de Ciencias, Universidad de la República, Uruguay.

*Correspondence to : p.chaboche@protonmail.com

Abstract

Atmospheric nuclear tests (1945–1980) have led to radioactive fallout across the globe. French tests in Polynesia (1966–1974) may influence the signature of fallout in South America in addition to those conducted by USA and former USSR until 1963 in the Northern hemisphere. Here, we compiled the $^{240}\text{Pu}/^{239}\text{Pu}$ atom ratios reported for soils of South America and conducted additional measurements to examine their latitudinal distributions across this continent. Significantly lower ratio values were found in the 20–45° latitudinal band (0.04 to 0.13) compared to the rest of the continent (up to 0.20) and attributed to the contribution of the French atmospheric tests to the ultra-trace plutonium levels found in these soils. Based on sediment cores collected in lakes of Chile and Uruguay, we show the added value of measuring $^{240}\text{Pu}/^{239}\text{Pu}$ atom ratios to refine the age models of environmental archives in this region of the world.

Keywords: Plutonium isotopes, Nuclear weapon tests, Geochronology, Soil erosion

44 1. Introduction

45 Anthropogenic radionuclides emitted by atmospheric nuclear weapon tests (NWT)
46 conducted after 1945 have been widely used as powerful markers to date environmental archives
47 and conduct climatic and environmental reconstructions (Alewell et al., 2017; Foucher et al., 2021;
48 Hancock et al., 2011; Ritchie and Ritchie, 2007). This information is also used both to reconstruct
49 soil erosion rates during the Great Acceleration (Steffen et al., 2015) – the period that started in
50 1950 and that is characterised by a general increase of the human imprint on global biogeochemical
51 cycles – and for sediment source fingerprinting research (Evrard et al., 2020; Meusburger et al.,
52 2016). Over 90% of the total energy yield (440 Mt) associated with NWT was detonated in the
53 Northern hemisphere, during tests that were mainly carried out by the United States (US) until
54 1958 in the Marshall Islands and then by the Former Soviet Union (FSU) between 1961 and 1962
55 at the Novaya Zemlya and Semipalatinsk sites (UNSCEAR, 2008). The opening to the signature
56 of the Partial Test-Ban Treaty on August 5, 1963 has significantly reduced global emissions of
57 artificial radionuclides into the environment, with the end of the atmospheric tests conducted by
58 the USA, FSU and the United Kingdom (UK). After initial tests in the Saharan Desert (1960–1966),
59 France conducted most of its nuclear experiments at the *Centre d'Expérimentation du Pacifique*
60 (C.E.P) in Polynesia, with 41 atmospheric tests conducted in the vicinity of Moruroa and
61 Fangataufa atolls between 1966 and 1974. In the Northern Hemisphere, China carried out
62 atmospheric tests in Lop Nor until 1980 (Fig. 1).

63 <Figure 1 here>

64 Depending on the type of test, its yield, firing altitude and latitude, radioactive debris
65 attached to ambient aerosol particles were distributed between the troposphere and the stratosphere.
66 Tropospheric debris were dispersed within the latitude band of the initial injection and followed
67 wind-driven trajectories, before being deposited onto the soil or ocean surfaces with residence
68 times comprised between 30-70 days (Bennett, 2002; Holloway and Hayes, 1982). Stratospheric
69 deposition across the world accounts for the majority of global long-lived fission product residues,
70 with atmospheric residence times comprised between 3 and 24 months depending on whether the
71 debris were injected in the polar or the equatorial regions (UNSCEAR, 2000). In addition to the
72 ubiquitous ^{137}Cs ($T_{1/2} = 30$ years) found across the globe, the analysis of plutonium (Pu) isotopes
73 including ^{239}Pu ($T_{1/2} = 24\ 110$ years) and ^{240}Pu ($T_{1/2} = 6\ 561$ years) offer the opportunity to
74 discriminate between contrasted sources of radionuclides in general, and Pu in particular. Based on
75 the available worldwide compilations, it is currently accepted that the deposition of ^{137}Cs and
76 $^{239+240}\text{Pu}$ reached a peak in 1963 and 1964-1965 in the Northern and Southern hemispheres,
77 respectively (Cambray et al., 1989; Turney et al., 2018). The delay observed between fallout peaks
78 is attributed to the time required for allowing exchanges of nuclear fallout products between both
79 hemispheres.

80 Although the fallout signatures associated with the tests conducted in the Northern
81 Hemisphere have received a significant interest, much less is known regarding the deposition that
82 took place in South America, e.g. in response to the nuclear tests conducted in the Southern
83 hemisphere. Although the devices tested were less powerful than those developed by the USA and
84 the FSU, the environmental impacts of the French nuclear experiments may have led to a distinct
85 labelling of soils and sediments across this subcontinent. Sources of radionuclides in this part of
86 the world are more limited, as they only include part of the emissions of the tests conducted by the
87 i) USA and the UK in equatorial regions (Pacific Proving Grounds) until 1962, ii) FSU in the Arctic,
88 and iii) those conducted by France in Polynesia in the late 1960s and the early 1970s. The situation

89 is also characterised by the lack of significant fallout in the Southern hemisphere following the
90 Chernobyl (1986) and Fukushima (2011) nuclear power plant accidents (Steinhauser et al., 2014).

91 The development of mass spectrometric techniques such as Inductively-Coupled Plasma
92 Mass Spectrometry (ICP-MS) and Accelerator Mass Spectrometry (AMS) offered the opportunity
93 to quantify ultra-trace levels of plutonium isotopes (fg to ag g⁻¹) in a variety of contrasted
94 environmental matrices (*e.g.* ice, soil, sediment, vegetation) after thorough chemical purifications.
95 Importantly, ICP-MS and AMS provided powerful techniques to quantify individually ²⁴⁰Pu and
96 ²³⁹Pu, which was not possible in previous studies relying on alpha spectrometry, providing only
97 the sum of both isotopes (²³⁹⁺²⁴⁰Pu).

98 Early records of radioactive fallout in the Southern hemisphere were derived from the
99 analysis of ice cores collected in Antarctica (Koide et al., 1985). Although they were collected at
100 ~75° latitude south (°S), *i.e.* in latitudinal bands far from those where France (22°S) or the USA
101 (near the Equator) conducted detonations, their analysis demonstrated a change in the ²⁴⁰Pu/²³⁹Pu
102 atom ratios with time. For example, the ratios found in ice deposited in the late 1950s dominated
103 by the US tests in the Pacific Proving Ground (0.19–0.34) were higher than those accumulated in
104 the early 1960s and dominated by the FSU tests (0.16–0.19), which indicates that Pu atom ratios
105 provide relevant indicators to monitor potential changes in sources of nuclear fallout.

106 To address controversies (Arnaud et al., 2006; Guevara and Arribére, 2007; Magand and
107 Arnaud, 2007) regarding the sources and the timing of radionuclide fallout at the scale of South
108 America, our study provides a novel compilation of already published and new original ²⁴⁰Pu/²³⁹Pu
109 atom ratio measurements conducted in soils and sediments collected across the subcontinent. As
110 previously hypothesized (Chamizo et al., 2011; Kelley et al., 1999), South America was, in addition
111 to global fallout following nuclear tests carried out in the Northern hemisphere, also partially
112 exposed to the fallout associated with nuclear tests performed in the Southern hemisphere, notably
113 the French nuclear tests conducted in Polynesia. To the best of our knowledge, this contribution
114 had never been calculated so far and its consequences for various research fields in Earth Science
115 (soil redistribution assessment, climatic and environmental reconstructions) would deserve the
116 discussion that is provided in the current research, given the potential of these analyses to refine
117 spatial and temporal interpretations derived from routine radionuclide measurements.

118

119 **2. Materials and Methods**

120

121 *2.1. Sample collection*

122 Detailed information regarding study site and sample collection are provided in the original
123 publications listed in Table 1.

124 Sediment core was collected in 2020 in the Rincón del Bonete (RDB-01, 31 cm long) reservoir
125 using a 63 mm Uwittec gravity corer equipped with a 1 meter PVC liner tube available at the
126 Universidad de la República (Montevideo, Uruguay). Coring site was selected on the vicinity of
127 the dams in order to ensure the maximum accumulation of fine sediment.

128 Another 83 cm long sediment core (CG02, S 18°15.110', W 69°09.784') was collected in the
129 western basin of Lake Chungará (Chile) in October 2014 at a water depth of 29.4 m, using a
130 UWITEC gravity corer. Core opening and slicing were performed on the lake shore right after core
131 collection to avoid transport-related disturbance. Detailed information for core sampling and
132 processing are provided elsewhere (Guédron et al., 2019).

133
134
135
136
137
138
139
140
141
142
143
144
145
146
147
148
149
150
151
152
153
154
155
156
157
158
159
160
161
162
163
164
165
166
167
168
169
170
171
172
173
174
175
176
177

2.2. Gamma spectrometry

Prior to gamma spectrometry measurements, samples were dried at 40°C for at least 24 h, ground and passed through a 2 mm sieve, then placed in plastic Marinelli beakers. Gamma-ray measurements of ^{137}Cs (662 keV) in all samples were obtained using very low-background and high purity germanium detectors (HPGe) (Canberra) at Laboratoire des Sciences du Climat et de l'Environnement (LSCE, Gif-sur-Yvette, France) and the Laboratoire Souterrain de Modane (LSM, Modane, France). After quantification, ^{137}Cs activities (Bq kg^{-1}) were decay-corrected to 2020 assuming a decay constant of ^{137}Cs $\lambda = \text{Ln}2/30.2 \text{ y}$.

The $^{210}\text{Pb}_{\text{xs}}$ activities ($T_{1/2} = 22.3$ years) were calculated by subtracting the supported activity (determined by using two ^{226}Ra daughters), ^{214}Pb activities (average count number at 295.2 and 351.9 keV) and ^{214}Bi activity (609.3 keV) from the total ^{210}Pb activity measured at 46.5 keV.

Sample preparation and purification procedure for plutonium analysis

The sample preparation and isotope composition measurements for samples collected in Lake Chungará and Rincón del Bonete reservoir were carried in the analytical expertise laboratory (Arpajon, France) of the Military Application Division (DAM) of the French Atomic Energy Commission (CEA). All acids used were of analytical grade and one or two process blanks were prepared under the same conditions as the samples. Dissolution, separation and purification of Pu followed a procedure almost similar than described in previous publications (Evrard et al., 2014; Jaegler et al., 2018). Quantities of approximately 5 g of each sample were transferred to Pyrex® beakers, covered with watch glasses to prevent cross contamination and dry-ashed at 450 °C for ~ 15 h in an electric furnace to decompose organic matter. After cooling to room temperature, limited amount of ^{244}Pu (~1 pg) was added as an isotopic dilution tracer for plutonium quantitative analysis. Digestion of the samples was carried out through five successive acid leaching steps: one leaching with concentrated HNO_3 (30 mL), one leaching with fuming HNO_3 and H_2O_2 (1 mL during the second leaching), one leaching with concentrated HCl (30 mL) and a last one with 4 mol L^{-1} HCl (50 mL). It should be noted that between each leaching step, the solutions were back flow heated at 120-150°C for several hours before being evaporated to dryness using hot plates. Samples were then filtrated with a disposable 0.45 μm Nalgene filtering unit (Thermo Scientific, Rochester, NY, USA). Dissolved fractions were evaporated to dryness before being recovered with 8 mol L^{-1} HNO_3 (30 mL). Insoluble fractions were treated separately and transferred in clean Savillex® PFA Teflon® beakers, where a first digestion for 1 h with HF (20 mL) was done. Then, concentrated HNO_3 (5 mL) was added, followed by evaporation to dryness. Samples were recovered with HF (5 mL) and concentrated HNO_3 (20 mL) and evaporated to dryness. Samples were finally recovered with concentrated HNO_3 (25 mL) and H_2O_2 (1 mL), evaporated to dryness and recovered with 10 mL of 8 mol L^{-1} HNO_3 , before being added to the previous dissolved fractions and evaporated to dryness. Samples were recovered with 50 mL of 8 mol L^{-1} HNO_3 , and a few mg of $\text{NH}_2\text{OH.HCl}$ and NaNO_2 were added to stabilize the (+IV) oxidation state of Pu and evaporated to dryness. Samples were finally recovered with 50 mL of 8 mol L^{-1} HNO_3 before Pu separation on chromatographic columns.

Plutonium purification was performed with a 20 mL-column filled with Dowex AG1x8 anion-exchange resin (50-100 mesh AG1X8 and 100-200 mesh AG1X8 resins, 10 mL each), rinsed twice and conditioned with 60 mL of 8 mol L^{-1} HNO_3 . A second purification was carried out with a 2 mL-column filled with a Dowex AG1X4 anion-exchange resin (100-200 mesh resin). Samples were loaded in both columns, washed with 8 mol L^{-1} HNO_3 , 10 mol L^{-1} HCl and concentrated HCl

178 before Pu fraction elution with a NH_4I (1.5%)- 12 mol L^{-1} HCl solution. A succession of
179 evaporation to dryness and recovering was performed using concentrated HNO_3 . Finally, samples
180 were recovered with 3 mL of 2% HNO_3 for ICP-MS measurements.

181 Sample preparation and isotope composition measurements for soils located in the
182 Conceição River catchment (Brasil), in Antarctica and Peru were carried in the Laboratoire de
183 Métrologie de la Radioactivité dans l'Environnement (LMRE) of the Institut de Radioprotection et
184 de Sécurité Nucléaire (IRSN). Sample preparation was described in detail in previous papers and
185 includes a two-step procedure allowing quantification of ^{238}Pu and $^{239+240}\text{Pu}$ by alpha spectrometry,
186 then separately ^{239}Pu and ^{240}Pu by SF-ICP-MS (Bouisset et al., 2021). Acids used were analytical
187 grade for alpha spectrometry measurements, and superior quality for SF-ICP-MS. In summary,
188 approximately 50g of samples were ashed and spiked with ^{242}Pu (NIST SRM 4334). Digestion of
189 the samples was carried out during 4 days using HNO_3 , HCl and H_2O_2 , followed by three successive
190 coprecipitations of actinides. Plutonium separation was then performed using chromatography
191 column with anion exchange resin AG1X8 (Bio-rad), conditioned in 8 mol L^{-1} HNO_3 , and eluted
192 with 12 mol L^{-1} $\text{HCl}/0.1$ mol L^{-1} NH_4I . The purified fraction containing Pu was evaporated, before
193 being dissolved in concentrated HNO_3 and prepared by electrodeposition onto stainless steel discs
194 (cathode) and Pt (anode). Pu isotopes were measured during 14 days with a low level background
195 alpha spectrometer (alpha-analyst, Canberra) with 450 mm^2 PIPS detectors and using Genie 2000
196 software (Canberra). Then, Pu electroplated samples were dissolved with concentrated HNO_3 and
197 HCl . The solution was evaporated and recovered with 8 mol L^{-1} HNO_3 . NaNO_2 was added for
198 valence adjustment of Pu to Pu(IV). Plutonium purification was performed using a column filled
199 with a Dowex AG1X8 anion-exchange resin and 8 mol L^{-1} HNO_3 before being eluted with HCl/HI .
200 Finally, samples were evaporated to dryness and recovered with 0.5 mol L^{-1} HNO_3 for ICP-MS
201 measurements.

202

203 *2.3. Isotope composition measurements by multiple-collector ICP-MS*

204 Pu isotopic composition for samples collected in Lake Chungará and Rincón del Bonete
205 reservoir were measured with a Multi-Collector ICP-MS ("Neptune Plus", Thermo Fisher
206 Scientific Inc., Bremen, Germany) equipped with eight Faraday cups and five ion counters. Ions
207 counters were used for simultaneous measurements of plutonium isotopes (^{239}Pu , ^{240}Pu , ^{241}Pu ,
208 ^{242}Pu , ^{244}Pu). Faraday cups were used to monitor uranium content (^{238}U , to correct for ^{238}U hydrides
209 and peak tailing) and lead content (to correct for PbO_2 interferences). An Aridus II (Cetac) as an
210 introduction system, high efficiency sampler and skimmer cones, and a reinforced pumping in the
211 interface were implemented to enhance the sensitivity (by approximately a factor of 10 with respect
212 to the standard configuration). Two certified isotopic reference materials were used in ICP-MS
213 measurements (SRM-947, SRM-948) for mass bias correction and plutonium isotopic verification.

214

215 For samples collected in Antarctica, Conceição (Brasil) and Peru, measurements were made
216 with a sector field ICP-MS (SF-ICP-MS, Element 2, Thermo Fisher Scientific Inc., Bremen,
217 Germany). The introduction system was made up of a PFA MicroFlow nebulizer (200 $\mu\text{L}/\text{min}$)
218 connected to a high sensitivity desolvating system (apex Ω , ESI) and a cyclonic spray chamber
219 (PC3 – ESI). A high capacity dry interface pump and a set of cones (Jet Interface) were used to
220 enhance the sensitivity. Two reference material were used in alpha spectrometry and ICP-MS
221 measurements (IAEA-410 – Bikini atoll sediment and IAEA-412 – Pacific Ocean sediment)

222

223 2.4. Two-sources un-mixing model

224 The fraction of plutonium originating from a source with a much lower $^{240}\text{Pu}/^{239}\text{Pu}$ atom
225 ratio likely associated with French nuclear weapon tests (FNT) in the analysed samples was
226 estimated as the first source in an empirical two-sources un-mixing. The second source being the
227 global fallout (GF) associated with the pre-moratorium NWT. This model had been previously
228 used to evaluate the contribution of fallout from two sources, where both GF and local/regional
229 fallout have occurred on a given site (Kelley et al., 1999; Pittauer et al., 2017; Tighe et al., 2021).
230 The compilation of $^{240}\text{Pu}/^{239}\text{Pu}$ atom ratios published in the literature and the use of this two-
231 sources un-mixing model was used to identify those latitudinal bands with atom ratios differing
232 from the average global fallout signature.

233 Assuming that the $^{240}\text{Pu}/^{239}\text{Pu}$ atom ratio determined in one sample (R_S) is a mixture of both
234 fallout sources, the first with a low $^{240}\text{Pu}/^{239}\text{Pu}$ atom ratio (R_{FNT}) and the second with a ratio
235 corresponding to that of the global fallout (R_{GF}):

$$236 R_S = \chi_{\text{FNT}} \times R_{\text{FNT}} + (1 - \chi_{\text{FNT}}) \times R_{\text{GF}} \quad (\text{Eq. 1})$$

237 where χ_{FNT} and $1 - \chi_{\text{FNT}}$ are respective contributions of FNT and GF. Consequently, the proportion
238 of plutonium originating from this source with a much lower $^{240}\text{Pu}/^{239}\text{Pu}$ atom ratio, likely
239 associated with FNT, is calculated according to Eq. 2:

$$240 \chi_{\text{FNT}} = \frac{R_S - R_{\text{GF}}}{R_{\text{FNT}} - R_{\text{GF}}} \quad (\text{Eq. 2})$$

241 The standard-uncertainty of the contribution $u(\chi_{\text{FNT}})$ is determined by the combination of
242 uncertainties associated with each variable in Eq. 2 and is expressed as follows:

$$243 u(\chi_{\text{FNT}}) = \chi_{\text{FNT}} \times \sqrt{\left(\frac{u(R_S)}{R_S - R_{\text{GF}}}\right)^2 + \left(\frac{u(R_{\text{FNT}})}{R_{\text{FNT}} - R_{\text{GF}}}\right)^2 + \left(\frac{(R_S - R_{\text{FNT}}) \times u(R_{\text{GF}})}{(R_S - R_{\text{GF}}) \times (R_{\text{FNT}} - R_{\text{GF}})}\right)^2} \quad (\text{Eq. 3})$$

244 The R_{GF} signatures were previously determined from a worldwide survey in terrestrial soils
245 conducted between 1970-1971 by the Environmental Measurements Laboratory (EML) (Hardy et
246 al., 1973; Krey et al., 1976) and analysed by TIMS (Thermal ionization mass spectrometry) for Pu
247 atom ratio in the late 2000s (Fig. 2) (Kelley et al., 1999). Of note, radioactive fallout derived from
248 the Chinese and French nuclear tests conducted after the sampling period could therefore not be
249 recorded in these soil samples. In particular, approximately half of the tropospheric and
250 stratospheric fallout associated with the FNT occurred after the sampling period. According to
251 Kelley et al. (1999), R_{GF} is defined as 0.178 ± 0.019 , 0.173 ± 0.027 and 0.185 ± 0.047 for the 0-
252 10°N , $0-30^\circ\text{S}$ and $30-53^\circ\text{S}$ regions, respectively. Owing to the fact that uncertainties associated
253 with these values take into account FNT (in particular the $30-53^\circ\text{S}$ regions), we assume that a R_{GF}
254 signature of 0.179 ± 0.010 is representative of the radionuclide fallout associated with the USA,
255 FSU and UK tests at the scale of South America.

256 Most information published regarding R_{FNT} in tropospheric fallout is based on the analyses
257 conducted on samples collected in 1996 by the International Atomic Energy Agency (IAEA),
258 where a $^{240}\text{Pu}/^{239}\text{Pu}$ atom ratio of 0.04 ± 0.01 can be estimated for samples collected in Fangataufa
259 atoll where part of the French tests was conducted (see the Discussion section). For R_S values

260 greater than R_{GF} , it is assumed that the Pu is fully derived from GF with corresponding
261 contributions equal to 100%.

262 3. Results

263

264 3.1. Spatial extent of plutonium signatures in soils

265 Uncertainties and/or standard deviations associated with Pu ratios presented in this section
266 are detailed in Table 1.

267 The $^{240}\text{Pu}/^{239}\text{Pu}$ atom ratios published in the literature and determined in the current
268 research for four additional surface soil samples (0-5 cm) and two undisturbed soil profiles are
269 displayed in Table 1 and in Fig. 2. Overall, $^{240}\text{Pu}/^{239}\text{Pu}$ atom ratios remain rather heterogeneous
270 across South America, ranging from 0.041 ± 0.003 to 0.2045 ± 0.0046 with three distinct latitudinal
271 patterns. For the equatorial latitudes (10°N - 7°S), $^{240}\text{Pu}/^{239}\text{Pu}$ atom ratios in surface soils and
272 undisturbed soil profiles are characteristic of the average global fallout signature (~ 0.18 , Fig. 2).
273 Although information is scarce for the Southern part of the continent (latitude below 43°S), a
274 similar pattern is observed in these regions although Pu atom ratios were found to be slightly higher
275 in surface soils of Antarctica (0.19 ± 0.01), with a maximum $^{240}\text{Pu}/^{239}\text{Pu}$ atom ratio of $0.2045 \pm$
276 0.0046 observed in a soil profile from Punta Arenas, Chile (53°S , Fig. 2).

277 <Figure 2 here>

278 In contrast, the $^{240}\text{Pu}/^{239}\text{Pu}$ atom ratios found in soils located between 20 and 42°S on both
279 sides of the Andean Cordillera significantly deviate from the average global fallout signature (Fig.
280 2), with the lowest $^{240}\text{Pu}/^{239}\text{Pu}$ atom ratio (0.0041 ± 0.003) found at 33°S in a surface soil sample
281 of La Parva (Chile) (Chamizo et al., 2011). From this location, $^{240}\text{Pu}/^{239}\text{Pu}$ atom ratios found in
282 surface soils gradually increased southwards and northwards to reach the average global signature
283 in Southern and Northern Chile. Compared to the signatures found in other soil profiles of South
284 America, those obtained in Santiago, Chile, and Buenos Aires, Argentina, differ from the integrated
285 fallout signature for the 30 - 53°S regions (0.185 ± 0.047) (Kelley et al., 1999), with $^{240}\text{Pu}/^{239}\text{Pu}$
286 atom ratios of 0.116 ± 0.02 and 0.108 ± 0.001 , respectively (Table 1). In addition to the Buenos
287 Aires sample collected on the Atlantic coast, the undisturbed soil profiles collected from the
288 Conceição catchment (28°S , Brazil) analysed in the current research showed $^{240}\text{Pu}/^{239}\text{Pu}$ atom
289 ratios remaining homogeneous with depth (0.135 ± 0.006), while being slightly lower than those
290 found in the two soil profiles analysed by Kelley et al. (1999) in Rio de Janeiro (0.168 ± 0.003)
291 and Angra dos Reis (0.178 ± 0.002) located further North in Brazil (23°S).

292 <Table 1 here>

293 3.2. Respective contributions of global vs. French fallout (FF) in soils

294 The proportion of plutonium originating from the FNT, calculated from the two-source un-
295 mixing model (see section 2.5.), is provided in Table 1 and displayed in Fig. 3. Accordingly, the
296 highest contributions of FNT were calculated for surface soil samples collected on the western
297 continental margin of South America, in La Parva ($99.3 \pm 7.5\%$, 33°S) and Chillan ($48.8 \pm 7.7\%$,
298 36°S) both located in Chile (Fig. 3). In undisturbed soil profiles, the proportion increased between
299 23°S to 35°S from $8.0 \pm 6.8\%$ in Rio de Janeiro, Brazil, to $51.3 \pm 5.1\%$ in Buenos Aires, Argentina.
300 On the contrary, the contribution of GF remained unambiguously the main source of Pu found in

301 soils located in the Northern and Southern parts of the subcontinent, with proportions generally
302 exceeding 80% (Fig. 3).

303 <Figure 3 here>

304 3.3. Temporal evolution of fallout signature in sediment core profiles

305 The $^{210}\text{Pb}_{\text{xs}}$ dating method was used to provide the chronology of two sedimentary
306 sequences collected in Lake Chungará (Chile, 18°S – 69°W) and in the Rincón del Bonete
307 Reservoir (Uruguay, 32°S – 56°W). The Constant Flux Constant Sedimentation (CF:CS) was
308 applied to determine $^{210}\text{Pb}_{\text{xs}}$ age models for these sediment cores (Bruel and Sabatier, 2020;
309 Goldberg, 1963; Krishnaswamy et al., 1971) (Table 2).

310 <Table 2 here>

311 For Lake Chungará, a mean sedimentation rate of $0.95 \pm 0.04 \text{ mm yr}^{-1}$ (1σ) over the top 10
312 cm was previously determined (Guédron et al., 2019). Samples from successive layers had to be
313 regrouped as there was not sufficient material to perform high temporal-resolution analyses.
314 Plutonium isotopes were measured for three samples covering the periods 1908-1955 (5.75 – 9.75
315 cm), 1955-1987 (2.75-5.25 cm) and 1987-2014 (2.75-0 cm) according to the CF:CS model (see
316 Supplementary Fig. S1). The $^{240}\text{Pu}/^{239}\text{Pu}$ atom ratio gradually decreased with time from $0.252 \pm$
317 0.015 (1908-1955) to 0.127 ± 0.013 between 1987-2014 (proportion from FNT, $37.3 \pm 10.7\%$).
318 Sample CG6-11 corresponding to sediment deposited between 1955-1987, where the maximum
319 activity peaks of ^{137}Cs were detected, showed a $^{240}\text{Pu}/^{239}\text{Pu}$ atom ratio of 0.156 ± 0.009 (FNT: 16.3
320 $\pm 8.9\%$) (Fig. 4).

321 <Figure 4 here>

322 Higher down-core resolution with depth was available for the sediment core collected in
323 the Rincón del Bonete Reservoir, in Uruguay (Fig. 5). Importantly, sampling reached the bedrock
324 material and it was therefore assumed to cover the entire sedimentation period since the reservoir
325 has become operational early in the 1950s. In contrast, the CF:CS model applied to the $^{210}\text{Pb}_{\text{xs}}$
326 activities calculated a mean accumulation rate of $11.03 \pm 1.31 \text{ mm yr}^{-1}$ (1σ) over the uppermost 30
327 cm, which indicated that this sediment was deposited since 1991 ± 4 years onwards (see Fig. S2).
328 The $^{240}\text{Pu}/^{239}\text{Pu}$ atom ratios showed the occurrence of uniform values with depth, ranging from
329 0.082 to 0.107 with an average signature of 0.092 ± 0.015 , indicating a mean contribution of 62.2
330 $\pm 12.2\%$ from FNT in this sediment core.

331 <Figure 5 here>

332

333 4. Discussion

334

335 4.1. Signatures and spatial extent of French radioactive debris

336 The complete cessation of nuclear weapon testing by France took place in January 1996
337 following a final series of six underground tests conducted in Polynesia. The IAEA was mandated
338 on the same year to assess the radiological situation at the C.E.P (IAEA, 1998). Approximately 300

339 samples were collected in contrasted matrices (e.g. corals, soil profiles, aerosols, etc.) and analysed
340 for their content in ^{238}Pu , $^{239+240}\text{Pu}$ and ^{241}Am . Based on this survey, it was concluded that most of
341 the residual radioactivity in both atolls was derived from safety trials and barge tests, which have
342 led to significant local fallout. Then, in 2005, part of these samples was analysed by means of
343 AMS, and $^{240}\text{Pu}/^{239}\text{Pu}$ atom ratios characteristic of low yield detonations were observed (Hrnecek
344 et al., 2005) (see Table S1). In safety trial sites of Moruroa, a $^{240}\text{Pu}/^{239}\text{Pu}$ atom ratio of 0.019 was
345 determined, in close agreement with the signatures lower than 0.03 measured by Chiappini et al.
346 (1999) in lagoon sediments. In other areas of Moruroa atoll affected by detonations conducted on
347 barges, $^{240}\text{Pu}/^{239}\text{Pu}$ atoms ratios were found to be slightly higher and close to 0.05 in topsoils and
348 loose coral rocks (Chiappini et al., 1999; Hrnecek et al., 2005). For samples collected at Fangataufa
349 atoll, similar low $^{240}\text{Pu}/^{239}\text{Pu}$ atom ratio signatures of ~ 0.05 associated with the Rigel barge tests
350 (125 kT) conducted in 1966 were outlined in these studies. Recently, the contribution of close-in
351 fallout to the Pu deposition was investigated in Gambier Islands located 400 km south-east from
352 the C.E.P. The authors found an average $^{240}\text{Pu}/^{239}\text{Pu}$ atom ratios of 0.0394 ± 0.0062 in seven
353 undisturbed soil profiles (Bouisset et al., 2021).

354 With the exception of four devices detonated on barges and five safety trials conducted at
355 the soil surface, 34 atmospheric tests were carried out from balloons tethered at an altitude of
356 several hundred meters above the atolls. Of note, this type of device has been used to limit both
357 local and regional fallout in Polynesian regions, thereby injecting large proportions of fission
358 products into the upper troposphere or stratosphere depending on the yield. Despite the lack of
359 public information regarding individual signatures for these tests conducted in altitude, the
360 available data suggests that the $^{240}\text{Pu}/^{239}\text{Pu}$ atom ratios associated with the original low-yield
361 devices remained in the same range (0.03 – 0.07) as other weapon grade devices, such as those
362 detonated in Australia, Nevada Test Site and in the Pacific Proving Grounds by the UK and the
363 U.S (Froehlich et al., 2016; Hamilton et al., 2009; Hicks and Barr, 1984; Muramatsu et al., 2001;
364 Tims et al., 2013). In the light of the publicly available information, the R_{FNT} of 0.04 ± 0.01 used
365 in the un-mixing model previously described appears to be the most relevant to date.

366 Owing that a large proportion of FNT were conducted during the southern winter when a
367 dominant general circulation of air masses at mid-latitudes is characterised by West to East
368 directions (Cai et al., 2020), most of the radioactive particles injected into the troposphere
369 following kiloton explosions were likely first deposited in South America during the subsequent
370 days or weeks. This hypothesis is further supported by a set of declassified documents and maps
371 published by the French Ministry of Defence in 2013 regarding the spatial extent and trajectories
372 of radioactive clouds released from nuclear tests conducted by France in 1967 and 1968. In
373 addition, the low $^{240}\text{Pu}/^{239}\text{Pu}$ atom ratios observed in surface soils from La Parva (Chile) in
374 particular (ranging from 0.024 to 0.067, average 0.041 ± 0.003) (Chamizo et al., 2011), and in soils
375 located at similar latitudes as the C.E.P in general, strongly support the occurrence of direct
376 tropospheric fallout of FNT debris in these regions of South America.

377 In contrast, the contribution of stratospheric fallout from high-yield FNT to the Pu atom
378 ratios in soils cannot be estimated based on the current information available in the literature.
379 Information regarding the $^{240}\text{Pu}/^{239}\text{Pu}$ atom ratios signatures from stratospheric injections is more
380 limited and based on the analysis of air filters collected by the Health and Safety Laboratory
381 (HASL) from 1963 to 1970 at 40°S , 70°W between 10 and 16 km of altitude (Fig. 6). Similarly to
382 what can be observed in sediment cores analysed in the current research, the $^{240}\text{Pu}/^{239}\text{Pu}$ atom ratios

383 decreased from a GF signature (0.181 ± 0.005 , 1σ) between 1963 - 1966 to a lower signature (0.11
384 ± 0.02 , 1σ) in 1969-1970, which is in good agreement with those values reported for soils and
385 sediment cores collected at similar latitudes.

386 *4.2. Impact of plutonium signatures to improve sediment dating.*

387 Although not assessed in the current study, potential ^{137}Cs and plutonium mobility in
388 sediment cores has to be considered through additional analyses, such as grain size, mineralogy
389 and organic matter properties.

390 A plutonium isotopic signature characteristic of the high yield atmospheric tests conducted
391 in the 1950s by the US in the Pacific Proving Ground (Fig. 1) is observed in the lower part of the
392 Chungará sediment core with $^{240}\text{Pu}/^{239}\text{Pu}$ atom ratio of 0.252 ± 0.015 in sample CG12-20
393 (Muramatsu et al., 2001). According to the $^{210}\text{Pb}_{\text{xs}}$ age model, sample CG6-11 corresponds to
394 sediment deposited between 1955 and 1987, thereby reflecting the main radioactive fallout period
395 and containing fallout originating from tests conducted in both the Northern and Southern
396 hemispheres. The $^{240}\text{Pu}/^{239}\text{Pu}$ atom ratio of 0.156 ± 0.009 determined in this sample is in perfect
397 agreement with the signature proposed by Bouisset et al. (2021) for the Southern hemisphere (0.157
398 ± 0.011), including fallout from all the Nuclear Weapon States. A similar value was observed in
399 an undisturbed soil profile collected by the EML in Lima, Peru (0.1565 , 12°S), suggesting that
400 FNT debris, although they are less abundant, can also be observed in the Northern part of South
401 America (Fig. 3). The upward circulation that occurs in the equatorial regions (known as Hardley
402 circulation) has likely limited the deposition of FNT debris in these zones, as suggested by the
403 $^{240}\text{Pu}/^{239}\text{Pu}$ signature of ~ 0.18 determined in French Guiana and soil surface samples collected in
404 Peru in the framework of the current research. In contrast, the decreasing atom ratio observed in
405 sample CG1-5 (0.127 ± 0.013) for Lake Chungará sediments deposited between 1987-2014 is very
406 likely related to the higher proportion of FNT debris.

407 The $^{240}\text{Pu}/^{239}\text{Pu}$ atom ratios in sediment deposited in the Rincón del Bonete Reservoir,
408 although they are significantly lower than those measured in Lake Chungará, remained in
409 agreement with the plutonium signatures reported for undisturbed soil profiles collected at similar
410 latitudes by Kelley et al. (1999) (0.1156 ± 0.0017 and 0.1075 ± 0.0007 in Santiago and Buenos
411 Aires, respectively). The CF:CS $^{210}\text{Pb}_{\text{xs}}$ age model for this sediment core indicates sediment
412 accumulation since 1990. The analysis of $^{240}\text{Pu}/^{239}\text{Pu}$ atom ratios in this lacustrine archive
413 confirmed that the sampled sequence covered the most recent period (post-1990) when land use
414 change has dramatically modified sediment dynamics in this river catchment, with a brutal
415 transition from “pristine” natural grassland conditions to their conversion into cropland.
416 Considering the absence of a Pu signature characteristic of the 1964-1965 fallout peak, we
417 demonstrate the added value of analysing $^{240}\text{Pu}/^{239}\text{Pu}$ atom ratios in addition to ^{137}Cs and/or $^{210}\text{Pb}_{\text{xs}}$
418 in sediment profiles collected in this region of South America. This will avoid any age model
419 misinterpretation that may arise from an incorrect sediment dating from short-lived radionuclides
420 (see supplementary Fig. 2) or the lack of other local knowledge (e.g., regional land use changes).

421 *4.3. Wider implications*

422 South America has been exposed to significant land use change since the 1960s – a period
423 that coincides with that of the main radioactive fallout (Winkler et al., 2021). The conversion of
424 natural forests and grassland into cropland may result in the degradation of terrestrial ecosystems
425 and to an excessive sediment supply to lacustrine environments and river systems, as observed in

426 the Rincón del Bonete Reservoir. Accordingly, improving the chronology of this reconstruction is
427 of utmost interest in this part of the world. The current research demonstrates that the analysis of
428 $^{240}\text{Pu}/^{239}\text{Pu}$ ratios in addition to that of ^{137}Cs and $^{210}\text{Pb}_{\text{xs}}$ in lacustrine archives may contribute to
429 this ultimate objective given the strong spatial and temporal variations of this ratio compiled across
430 the continent and demonstrated in this study.

431 Low levels of ^{137}Cs analysed in soils and sediment of the Southern hemisphere outline the
432 need to find alternative chronomarkers to reconstruct soil redistribution rates and/or to cross-check
433 and validate the dating of sediment archives. Pu is a powerful candidate to achieve this goal as it
434 may allow further distinguishing between different time periods corresponding to contrasted
435 nuclear testing stages or fallout originating from nuclear experimentations carried out by different
436 countries based on the reconstruction of $^{240}\text{Pu}/^{239}\text{Pu}$ temporal evolution in sediment cores. The
437 $^{240}\text{Pu}/^{239}\text{Pu}$ atom ratio should therefore be analysed in sediment core layers showing a single or
438 multiple ^{137}Cs fallout peaks to avoid any misinterpretation in the core dating and, consequently, on
439 the chronology of the reconstruction of environmental processes that have occurred in this
440 subcontinent in general, and in the central part of South America in particular.

441 Models converting ^{137}Cs measurements (Mabit et al., 2014) into quantitative estimates of
442 erosional and depositional rates over the past decades are based on the assumption that radionuclide
443 fallout peaked in 1963. Based on the undisturbed soil profiles of Conceição, Brazil, we showed
444 that 30% of Pu deposition could be attributed to FNT at this site. Recalibrating these soil erosion
445 models for applications in mid-latitudes of South America (by shifting the fallout peak to the period
446 1965-1970 instead of 1963 as it is currently done) would better constrain soil redistribution rates
447 calculated in these regions.

448 In addition to the analysis of $^{240}\text{Pu}/^{239}\text{Pu}$ atom ratios, ^{238}Pu ($T_{1/2} = 88$ years) fallout peak in
449 1968, resulting from the atmospheric disintegration of a nuclear auxiliary power generator in 1964
450 (SNAP9-A), may provide an additional time marker (Hancock et al., 2011) to confirm the
451 occurrence of a radioactive fallout peak in 1970 in some regions of South America as suggested in
452 our study.

453 Accordingly, the current research encourages the scientific community to continue
454 analysing Pu in general, and $^{240}\text{Pu}/^{239}\text{Pu}$ atom ratios in particular, to improve our understanding of
455 the spatial distribution of Pu fallout and its chronology in the Southern Hemisphere. This improved
456 knowledge will undoubtedly provide a powerful anthropogenic marker that will contribute refining
457 the dating of sediment cores, with a focus on those processes that took place during the 1960s and
458 the 1970s when the conversion of natural areas into agricultural land increased around the world
459 in general, and in Southern America in particular.

460
461 **5. Conclusions**
462 A novel compilation of already published and new original plutonium isotopes ($^{239,240}\text{Pu}$)
463 measurements conducted in lake sediments and soils allowed us to update our knowledge of the
464 spatial and temporal distribution of artificial radioactive fallout in South America. Significantly
465 lower $^{240}\text{Pu}/^{239}\text{Pu}$ atom ratios differing from the average global fallout signature were found in the
466 20-45° latitudinal band and attributed to the higher contribution of the French atmospheric nuclear
467 weapon tests (1966-1974) to the deposition of plutonium in these soils and sediments. These results
468 indicate that fallout radionuclides from French atmospheric tests should be considered to avoid any

469 misinterpretation in sediment core dating and to refine the chronology of the reconstruction of
470 environmental processes in this region of the world.

471

472 **Acknowledgments**

473

474 Pierre-Alexis Chaboche received a PhD fellowship from the University of Versailles-Saint-
475 Quentin-en-Yvelines (a founding member of University Paris-Saclay). Collaboration between
476 France and Uruguay for sediment sampling is supported by an applied research project from the
477 Fondo Maria Viñas (FMV_1_2019_1_156244) funded by the National Agency of Research and
478 Innovation (ANII, Uruguay). The Antarctic samples were obtained thanks to a project of the
479 Instituto Antartico Uruguayo (IAU) (2015-2016). The authors thank the Laboratoire Souterrain de
480 Modane (LSM) facilities for the gamma spectrometry measurements.

481

482

483 **Competing interests:** The authors declare that they have no competing interests.

484

485 **Data and materials availability:** All data are available in the main text and/or the Supplementary
486 Materials.

487

488 **Author contributions:** P.A.C., O.E. and F.P. developed the research concepts. O.E., P.S., M.T.,
489 S.M., S.G., P.C., M.C. and G.C. collected the samples. P.A.C., O.E., F.P., P.S., A.F., T.T.,
490 J.M., M.T., A.H. and G.C. discussed the results and contributed to the redaction. P.A.C.
491 wrote the paper, O.E., F.P., P.S. and A.F. substantially revised it. P.A.C, A.H., B.B, C.C.,
492 P.S., M.T. and M.C. performed the analysis and measurements (radiochemistry, gamma
493 spectrometry and ICP-MS measurements). All authors revised the manuscript to prepare
494 the final version.

495

496

497

498

499

500

501

502

503

504

505

506

507

508

509

510

511

512

513

514

515

- 516
517
518 **References**
519
520 Alewell C, Pitois A, Meusburger K, Ketterer M, Mabit L. $^{239+240}\text{Pu}$ from “contaminant” to soil
521 erosion tracer: Where do we stand? *Earth-Science Reviews* 2017; 172: 107-123.
522 Arnaud F, Magand O, Chapron E, Bertrand S, Boës X, Charlet F, et al. Radionuclide dating (^{210}Pb ,
523 ^{137}Cs , ^{241}Am) of recent lake sediments in a highly active geodynamic setting (Lakes
524 Puyehue and Icalma—Chilean Lake District). *Science of the Total Environment* 2006; 366:
525 837-850.
526 Bennett BG. Worldwide dispersion and deposition of radionuclides produced in atmospheric tests
527 : Fallout from atmospheric nuclear tests : Impact on science and society. *Health Physics*
528 2002; 82: 644-655.
529 Bouisset P, Nohl M, Cossonnet C, Boulet B, Thomas S, Cariou N, et al. Contribution of close-in
530 fallout from the French atmospheric tests in inventories of Cs-137, Am-241 and plutonium
531 (238,239,240) in Gambier Islands (French Polynesia) - Signatures of stratospheric fallout
532 in the Southern Hemisphere. *Journal of Environmental Radioactivity* 2021; 235.
533 Bruel R, Sabatier P. serac: AR package for Shortlived RADionuclide Chronology of recent
534 sediment cores. *Journal of Environmental Radioactivity* 2020; 225: 106449.
535 Cai W, McPhaden MJ, Grimm AM, Rodrigues RR, Taschetto AS, Garreaud RD, et al. Climate
536 impacts of the El Niño–southern oscillation on South America. *Nature Reviews Earth &*
537 *Environment* 2020; 1: 215-231.
538 Cambray R, Playford K, Lewis G, Carpenter R. Radioactive fallout in air and rain: results to the
539 end of 1988. AERE R13575. Atomic Energy Authority, London, UK 1989.
540 Chamizo E, García-León M, Peruchena JI, Cereceda F, Vidal V, Pinilla E, et al. Presence of
541 plutonium isotopes, ^{239}Pu and ^{240}Pu , in soils from Chile. *Nuclear Instruments and Methods*
542 *in Physics Research Section B: Beam Interactions with Materials and Atoms* 2011.
543 Chiappini R, Pointurier F, Millies-Lacroix J, Lepetit G, Hemet P. $^{240}\text{Pu}/^{239}\text{Pu}$ isotopic ratios and
544 $^{239+240}\text{Pu}$ total measurements in surface and deep waters around Mururoa and Fangataufa
545 atolls compared with Rangiroa atoll (French Polynesia). *Science of the total environment*
546 1999; 237: 269-276.
547 Evrard O, Chaboche P-A, Ramon R, Foucher A, Lacey JP. A global review of sediment source
548 fingerprinting research incorporating fallout radiocesium (^{137}Cs). *Geomorphology* 2020:
549 107103.
550 Evrard O, Pointurier F, Onda Y, Chartin C, Hubert A, Lepage H, et al. Novel Insights into
551 Fukushima Nuclear Accident from Isotopic Evidence of Plutonium Spread along Coastal
552 Rivers. *Environmental Science & Technology* 2014; 48: 9334-9340.
553 Foucher A, Chaboche P-A, Sabatier P, Evrard O. A worldwide meta-analysis (1977–2020) of
554 sediment core dating using fallout radionuclides including ^{137}Cs and $^{210}\text{Pb}_{\text{xs}}$. *Earth System*
555 *Science Data Discussions* 2021: 1-61.
556 Froehlich M, Chan W, Tims S, Fallon S, Fifield L. Time-resolved record of ^{236}U and $^{239,240}\text{Pu}$
557 isotopes from a coral growing during the nuclear testing program at Enewetak Atoll
558 (Marshall Islands). *Journal of environmental radioactivity* 2016; 165: 197-205.
559 Goldberg ED. Geochronology with ^{210}Pb . *Radioactive dating* 1963: 121-131.
560 Guédron S, Tolu J, Brisset E, Sabatier P, Perrot V, Bouchet S, et al. Late Holocene volcanic and
561 anthropogenic mercury deposition in the western Central Andes (Lake Chungará, Chile).
562 *Science of The Total Environment* 2019; 662: 903-914.

563 Guevara SR, Arribère M. Comment on the article ‘Radionuclide dating (Pb-210, Cs-137, Am-241)
564 of recent lake sediments in a highly active geodynamic setting (Lakes Puyehue and
565 Icalma—Chilean Lake District)’. *Science of the Total Environment* 2007; 385: 310-311.

566 Hamilton T, Jernström J, Martinelli R, Kehl S, Eriksson M, Williams R, et al. Frequency
567 distribution, isotopic composition and physical characterization of plutonium-bearing
568 particles from the Fig-Quince zone on Runit Island, Enewetak Atoll. *Journal of*
569 *radioanalytical and nuclear chemistry* 2009; 282: 1019-1026.

570 Hancock G, Leslie C, Everett S, Tims S, Brunskill G, Haese R. Plutonium as a chronomarker in
571 Australian and New Zealand sediments: a comparison with ^{137}Cs . *Journal of*
572 *Environmental Radioactivity* 2011; 102: 919-929.

573 Hardy EP, Krey PW, Volchok HL. Global Inventory and Distribution of Fallout Plutonium. *Nature*
574 1973; 241: 444-445.

575 Hicks H, Barr D. Nevada test site fallout atom ratios: $^{240}\text{Pu}/^{239}\text{Pu}$ and $^{241}\text{Pu}/^{239}\text{Pu}$: Lawrence
576 Livermore National Laboratory, University of California, 1984.

577 Holloway RW, Hayes DW. Mean residence time of plutonium in the troposphere. *Environmental*
578 *Science & Technology* 1982; 16: 127-129.

579 Hrncsek E, Steier P, Wallner A. Determination of plutonium in environmental samples by AMS
580 and alpha spectrometry. *Applied Radiation and Isotopes* 2005; 63: 633-638.

581 IAEA. The radiological situation at the atolls of Mururoa and Fangataufa: main report: report.
582 Vienna: International Atomic Energy Agency, 1998.

583 Jaegler H, Pointurier F, Onda Y, Hubert A, Lacey JP, Cirella M, et al. Plutonium isotopic
584 signatures in soils and their variation (2011-2014) in sediment transiting a coastal river in
585 the Fukushima Prefecture, Japan. *Environmental Pollution* 2018; 240: 167-176.

586 Kelley JM, Bond LA, Beasley TM. Global distribution of Pu isotopes and ^{237}Np . *Science of The*
587 *Total Environment* 1999; 237-238: 483-500.

588 Koide M, Bertine KK, Chow TJ, Goldberg ED. The $^{240}\text{Pu}/^{239}\text{Pu}$ ratio, a potential geochronometer.
589 *Earth and planetary science letters* 1985; 72: 1-8.

590 Krey P, Hardy E, Pachucki C, Rourke F, Coluzza J, Benson W. Mass isotopic composition of
591 global fall-out plutonium in soil. *Transuranium nuclides in the environment*, 1976.

592 Krishnaswamy S, Lal D, Martin J, Meybeck M. Geochronology of lake sediments. *Earth and*
593 *Planetary Science Letters* 1971; 11: 407-414.

594 Mabit L, Zapata F, Dercon G, Benmansour M, Bernard C, Walling D. Assessment of soil erosion
595 and sedimentation: the role of fallout radionuclides. 2014.

596 Magand O, Arnaud F. Response on the comment from Ribeiro Guevara and Arribere on the article
597 ‘Radionuclide dating (Pb-210, Cs-137, Am-241) of recent lake sediments in a highly
598 geodynamic setting (Lakes Puyehue and Icalma—Chilean Lake District)’. 2007.

599 Meusburger K, Mabit L, Ketterer M, Park J-H, Sandor T, Porto P, et al. A multi-radionuclide
600 approach to evaluate the suitability of $^{239+240}\text{Pu}$ as soil erosion tracer. *Science of the Total*
601 *Environment* 2016; 566: 1489-1499.

602 Muramatsu Y, Hamilton T, Uchida S, Tagami K, Yoshida S, Robison W. Measurement of
603 $^{240}\text{Pu}/^{239}\text{Pu}$ isotopic ratios in soils from the Marshall Islands using ICP-MS. *Science of the*
604 *Total Environment* 2001; 278: 151-159.

605 Pittauer D, Tims SG, Froehlich MB, Fifield LK, Wallner A, McNeil SD, et al. Continuous transport
606 of Pacific-derived anthropogenic radionuclides towards the Indian Ocean. *Scientific reports*
607 2017; 7: 1-8.

608 Ritchie JC, Ritchie CA. Bibliography of publications of ¹³⁷Cesium studies related to erosion and
609 sediment deposition. USDA–ARS Hydrology and Remote Sensing Laboratory Occasional
610 Paper HRSL-2007-01. USDA–Agricultural Research Service, Beltsville, MD, USA 2007.

611 Steffen W, Broadgate W, Deutsch L, Gaffney O, Ludwig C. The trajectory of the Anthropocene:
612 the great acceleration. *The Anthropocene Review* 2015; 2: 81-98.

613 Steinhäuser G, Brandl A, Johnson TE. Comparison of the Chernobyl and Fukushima nuclear
614 accidents: a review of the environmental impacts. *Science of the total environment* 2014;
615 470: 800-817.

616 Tighe C, Castrillejo M, Christl M, Degueldre C, Andrew J, Semple KT, et al. Local and global
617 trace plutonium contributions in fast breeder legacy soils. *Nature communications* 2021;
618 12: 1-10.

619 Tims SG, Fifield LK, Hancock GJ, Lal RR, Hoo WT. Plutonium isotope measurements from across
620 continental Australia. *Nuclear Instruments and Methods in Physics Research Section B:
621 Beam Interactions with Materials and Atoms* 2013; 294: 636-641.

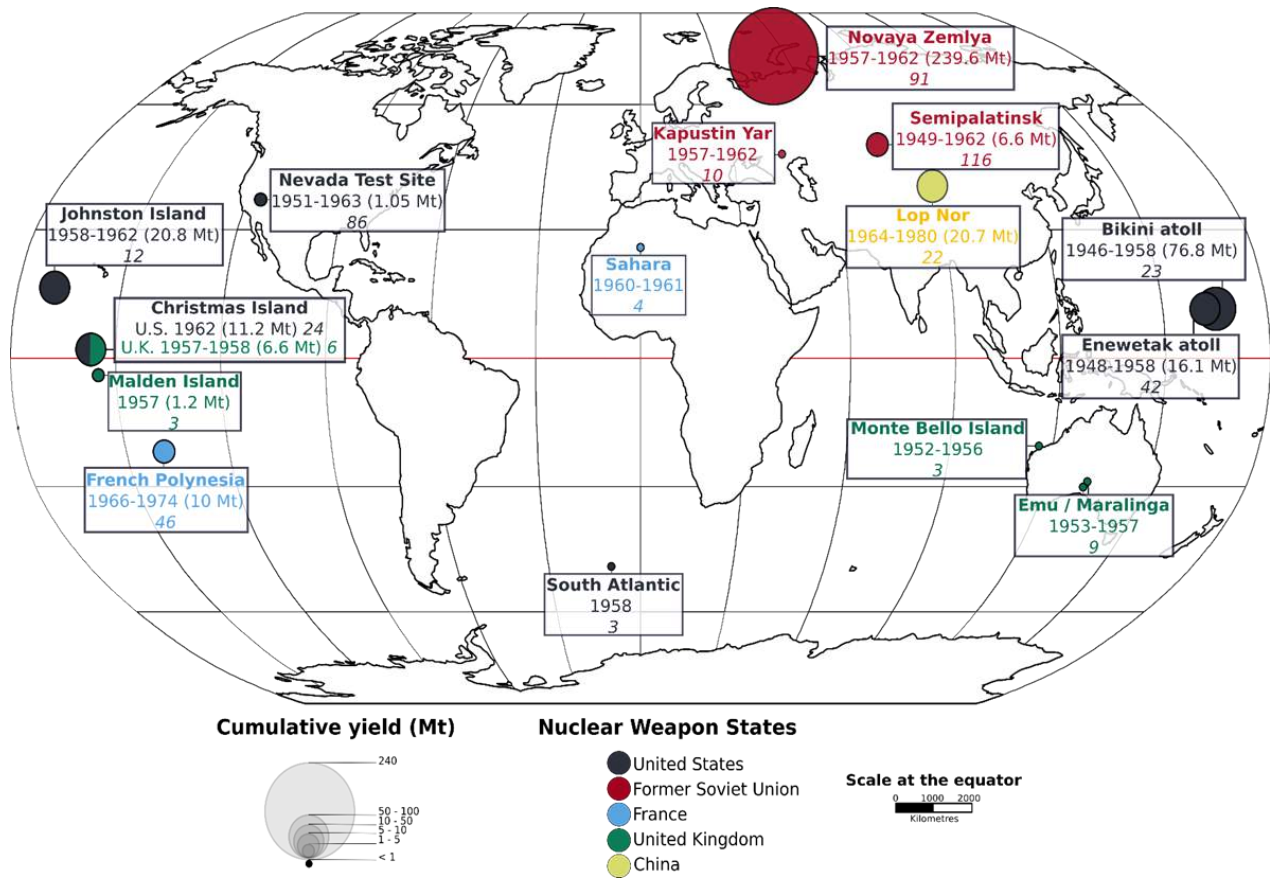
622 Turney CS, Palmer J, Maslin MA, Hogg A, Fogwill CJ, Southon J, et al. Global peak in
623 atmospheric radiocarbon provides a potential definition for the onset of the anthropocene
624 epoch in 1965. *Scientific reports* 2018; 8: 3293.

625 UNSCEAR. *Effects of Ionizing Radiation*. United Nations, New York 2000: 453-487.

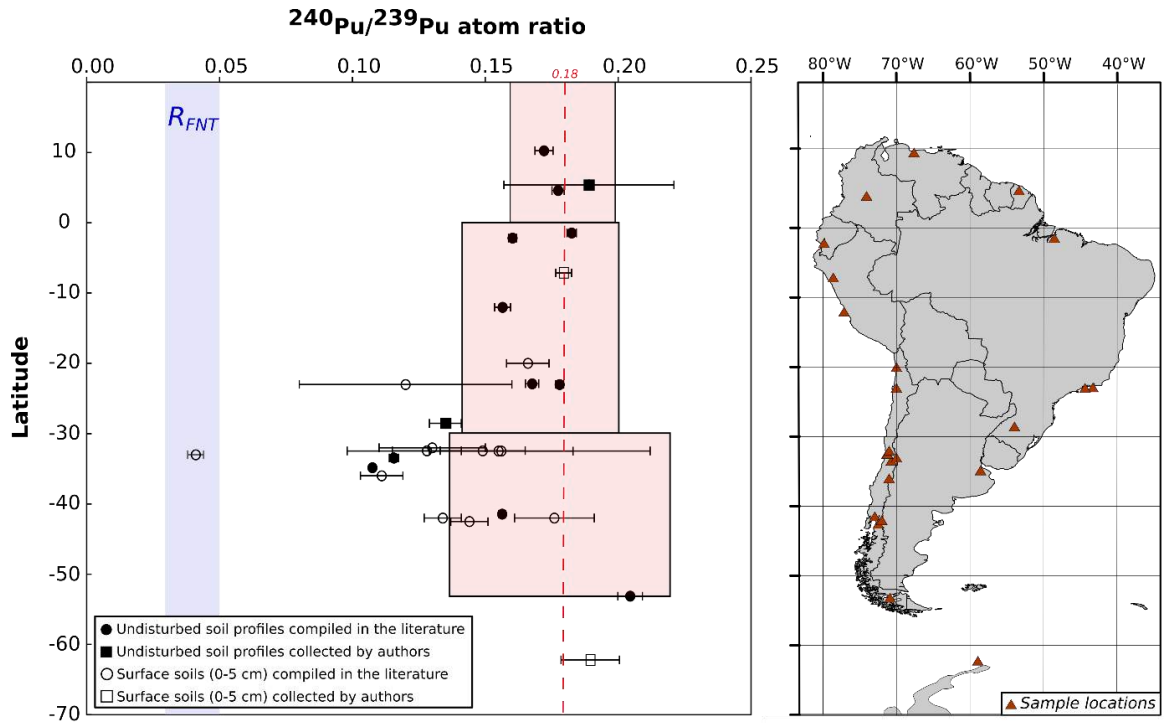
626 UNSCEAR. *Sources and effects of ionizing radiation: United Nations Scientific Committee on the
627 Effects of Atomic Radiation: UNSCEAR 2008 report to the General Assembly, with
628 scientific annexes*. New York: United Nations, 2008.

629 Winkler K, Fuchs R, Rounsevell M, Herold M. Global land use changes are four times greater than
630 previously estimated. *Nature communications* 2021; 12: 1-10.

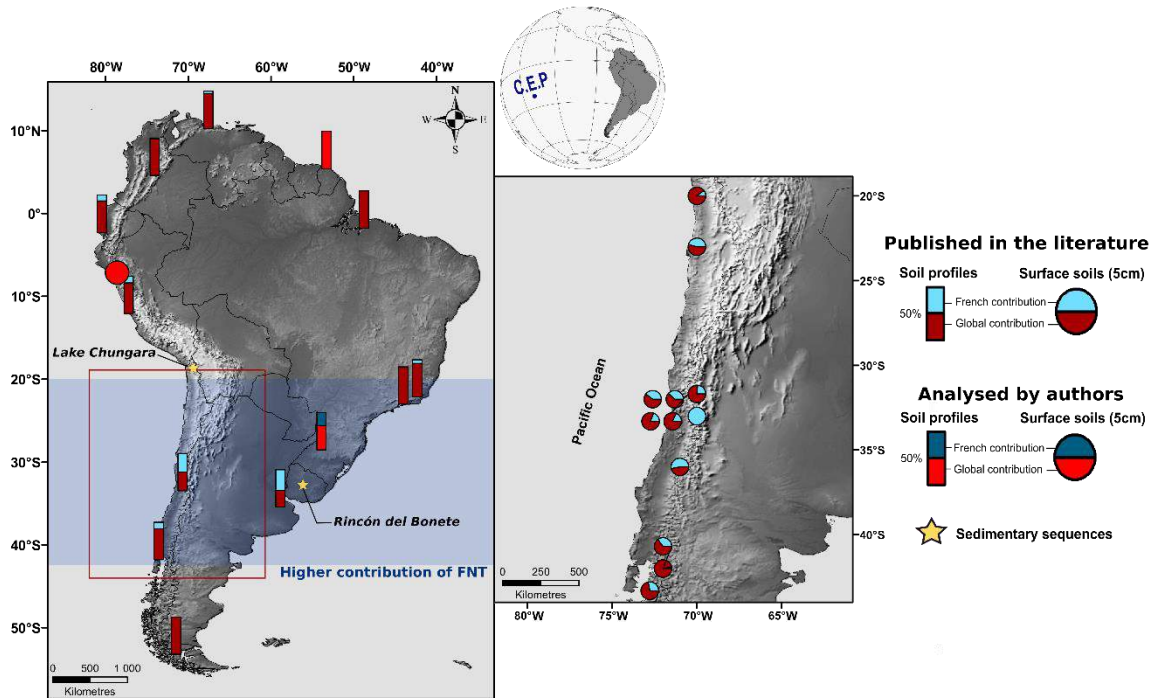
631
632
633
634
635
636
637
638
639
640
641
642
643
644
645
646
647
648
649
650
651
652
653
654



657
 658 **Fig. 1.** Location, timing, number (in italics) and total yield of atmospheric nuclear tests conducted
 659 around the world (8). Two operational nuclear detonations (Hiroshima, Nagasaki), 39 safety
 660 trials, four tests in the Pacific Ocean, one in New Mexico (USA) and two tests in Aralsk
 661 (Former Soviet Union) with a cumulative yield of approximately 0.2 Mt (0.045% of the
 662 total yield) are not shown for clarity.

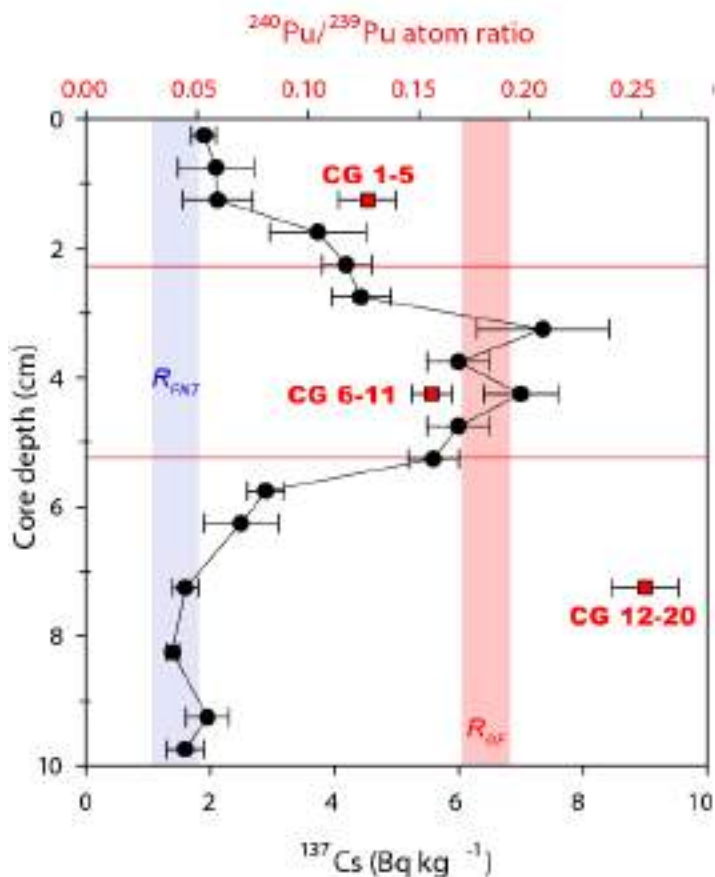


663
 664
 665 **Fig. 2.** Latitudinal distribution of $^{240}\text{Pu}/^{239}\text{Pu}$ atom ratios in undisturbed soil profiles and surface
 666 soils across continental South America and Antarctica published in the literature (circle)
 667 and analysed in the current research (square). The red rectangles indicate the integrated
 668 fallout signatures in different latitudinal ranges as determined from soils collected in 1970-
 669 1971 (19), while the blue rectangle (R_{FNT}) indicates the French fallout signature reported in
 670 previous studies. The average global fallout signature in soils (~ 0.18) is displayed as a red
 671 dashed line.
 672



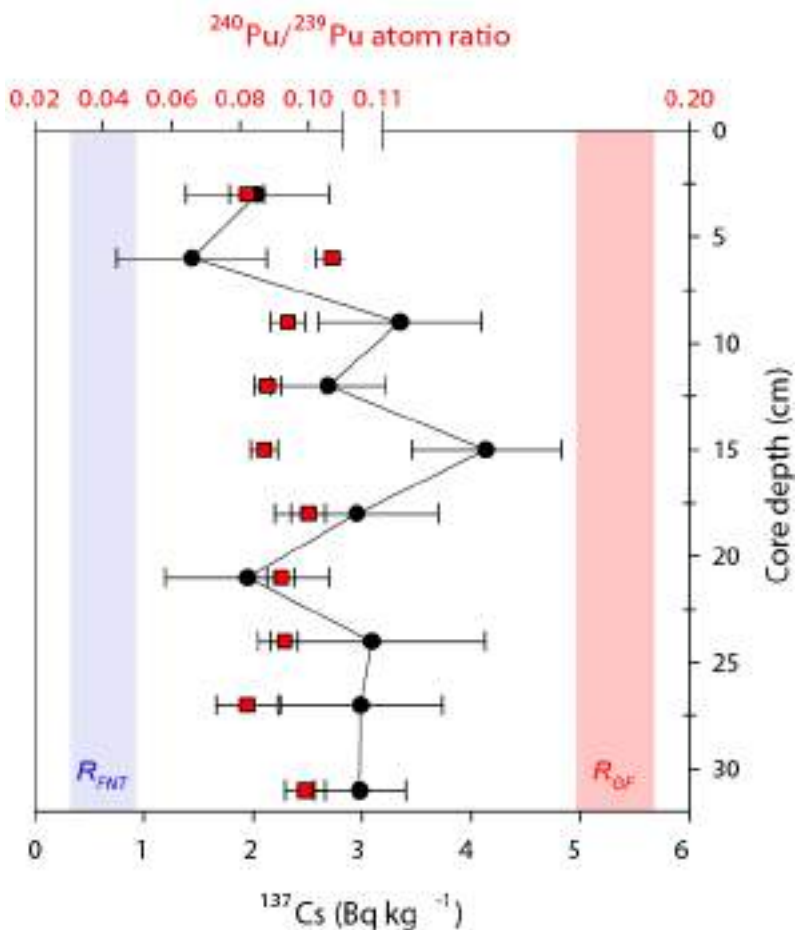
673
 674 **Fig. 3.** Respective contributions of global and French fallout in South America surface soil samples
 675 and undisturbed soil profiles published in the literature and analysed in the current research.
 676 Contribution uncertainties for each sample can be found in Table 1. Soil samples from
 677 Antarctica are not displayed for clarity. The location of the *Centre pour l'Expérimentation*
 678 *du Pacifique* (C.E.P.) is shown in the inset world map.
 679

Lake Chungara (18°S)

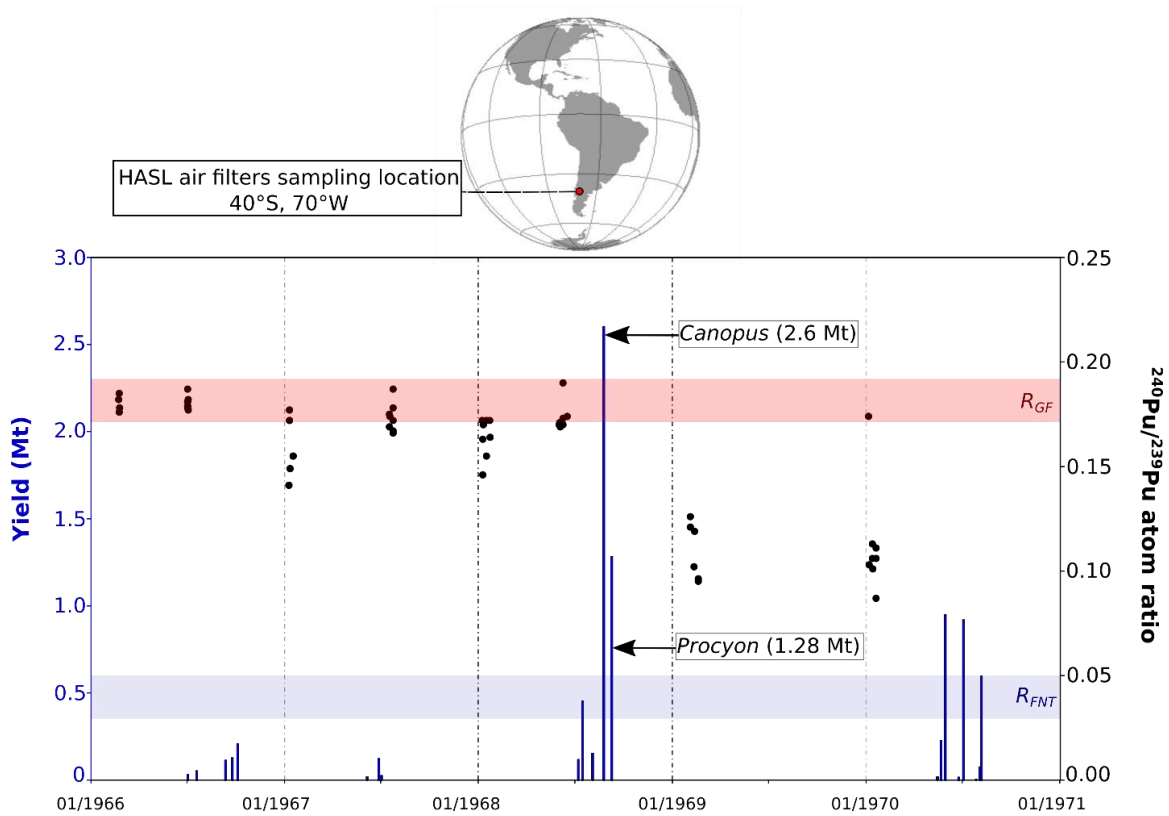


680
 681 **Fig. 4.** Temporal evolution of $^{240}\text{Pu}/^{239}\text{Pu}$ atom ratios (red squares) and ^{137}Cs activities (black dots)
 682 in sediment core collected in Lake Chungara (Chile). The French (R_{FNT} , in blue) and global
 683 (R_{GF} , in red) $^{240}\text{Pu}/^{239}\text{Pu}$ atom ratio fallout signatures used in the current research are
 684 provided as an indication.
 685

Rincón del Bonete (32°S)



686
 687
 688 **Fig. 5:** Temporal evolution of $^{240}\text{Pu}/^{239}\text{Pu}$ atom ratios (red squares) and ^{137}Cs activities (black dots)
 689 in sediment core collected in Rincón del Bonete reservoir (Uruguay). The French (R_{FNT} , in blue)
 690 and global (R_{GF} , in red) $^{240}\text{Pu}/^{239}\text{Pu}$ atom ratio fallout signatures used in the current
 691 research are provided as an indication. Please note the scale difference for reporting the
 692 $^{240}\text{Pu}/^{239}\text{Pu}$ atom ratios in the sediment core.
 693



694
 695 **Fig. 6.** $^{240}\text{Pu}/^{239}\text{Pu}$ temporal evolution in air filters collected by HASL between 1965 and 1971 at
 696 40°S latitude (black dots, no uncertainties for these samples were provided in the initial
 697 database), plotted along with French nuclear test yields over the same period. The R_{FNT} (in
 698 blue) and R_{GF} (in red) fallout signatures used in the current research are provided as an
 699 indication
 700

701
702
703
704
705
706
707

Table 1. ²⁴⁰Pu/²³⁹Pu atom ratios in soils of South America published in the literature and analysed in the current research. ^aSampling carried out in other studies and analysed for Pu isotopes by the authors; ^b²⁴⁰Pu/²³⁹Pu atom ratios as reported in Table 2 from Kelley et al., 1999; ^c"Weighted mean of duplicate aliquots from the same sample collection" (19); * Samples analysed at the IRSN; ** Samples analysed at the CEA/DAM.

Country	Latitude	Longitude	Study Area / Sample label	Elevation (m)	Sampling year	²⁴⁰ Pu/ ²³⁹ Pu	Proportion of Plutonium from French fallout	Measurement technique	Author	Note
French Guiana**	5.41	-53.31	ROC	84	2016	0.189 ± 0.032	0%	ICP-MS	de Tombeur et al., 2020 ^a	Undisturbed soil profile (0-40 cm) - Measurement ± 2σ error
Peru*	-7.13	-78.61	PASO02	3630	2017	0.178 ± 0.013	0.5 ± 11.7%	ICP-MS	This study	Surface soil (0-5cm)- Measurement ± 2σ error
Peru*	-7.14	-78.60	PASO05	3570	2017	0.181 ± 0.015	0%		This study	Surface soil (0-5cm)- Measurement ± 2σ error
Brazil*	-28.53	-53.92	CON 2-4cm	270	01/2016	0.132 ± 0.011	33.7 ± 9.5%	ICP-MS	Didoné et al., 2019 ^a	Undisturbed soil profile (0-42 cm) Measurement ± 2σ error
			CON 6-8cm			0.131 ± 0.011	34.4 ± 9.5%			
			CON 10-12cm			0.137 ± 0.012	30 ± 10.2%			
			CON 14-16cm			0.133 ± 0.011	32.9 ± 9.6%			
			CON 18-20cm			0.14 ± 0.016	27.9 ± 12.8%			
			Conceição average	/	/	0.135 ± 0.006	31.5 ± 6.9%			²⁴⁰ Pu/ ²³⁹ Pu = Average ± 2σ (n=5)
Antarctica*	-62.19	-58.91	A1	17	2017	0.195 ± 0.015	0%	ICP-MS	This study	Surface soil (0-5cm)- Measurement ± 2σ error
	-62.19	-58.91	A2	17	2017	0.184 ± 0.018	0%			This study
Published in the literature										
Venezuela	10.25	-67.6	Maracay S-1598	n.d.	10/1970 to 01/1971	0.1721 ± 0.0034	4.7 ± 7.2%	TIMS	Kelley et al., 1999 ^b	Undisturbed area sampled to a depth of 30cm Measurement ± 1σ error
Colombia	4.6	-74.08	Bogota S-1599	n.d.	10/1970 to 01/1971	0.1774 ± 0.00232 ^c	0.9 ± 7.2%			
Brazil	-1.45	-48.48	Belem S-1607	n.d.	10/1970 to 01/1971	0.1825 ± 0.00176	n.d.			
Equador	-2.17	-79.87	Guayaquil S-1627	n.d.	10/1970 to 01/1971	0.1602 ± 0.00151 ^c	13.3 ± 6.3%			
Peru	-12.02	-77.13	Lima S-1632	n.d.	10/1970 to 01/1971	0.1565 ± 0.003 ^c	16.0 ± 6.4%			
Brazil	-22.9	-43.23	Rio de Janeiro S-1728/9	n.d.	10/1970 to 01/1971	0.1676 ± 0.0025	8.0 ± 6.8%			
Brazil	-23	-44.3	Angra dos Reis S-1605	n.d.	10/1970 to 01/1971	0.178 ± 0.0015	0.5 ± 7.1%			
Chile	-33.45	-70.7	Santiago S-1708	n.d.	10/1970 to 01/1971	0.1156 ± 0.0017	45.5 ± 5.2%			
Argentina	-34.85	-58.53	Buenos Aires S-1642	n.d.	10/1970 to 01/1971	0.1075 ± 0.0007 ^c	51.3 ± 5.1%			
Chile	-41.45	-72.95	Puerto Montt S-1690	n.d.	10/1970 to 01/1971	0.1563 ± 0.0013 ^c	16.1 ± 6.1%			
Chile	-53.13	-70.88	Punta Arenas S-1707	n.d.	10/1970 to 01/1971	0.2045 ± 0.0046	0%			
Chile	-32.43	-71.24	La Greda	n.d.	From 2009 to 2010	0.149 ± 0.016	21.4 ± 12.9%	AMS	Salmani-Ghabeshi et al., 2018	Surface soil (0-5cm) - ²⁴⁰ Pu/ ²³⁹ Pu = Average ± 1σ (n=4)
Chile	-32.46	-71.27	Los Maitenes	n.d.	From 2007 to 2010	0.155 ± 0.057	17.1 ± 41.5%			Surface soil (0-5cm) - ²⁴⁰ Pu/ ²³⁹ Pu = Average ± 1σ (n=3)
Chile	-32.45	-71.28	Puchuncavi	n.d.	From 2007 to 2010	0.128 ± 0.013	36.5 ± 10.7%			Surface soil (0-5cm) - ²⁴⁰ Pu/ ²³⁹ Pu = Average ± 1σ (n=3)
Chile	-32.48	-71.26	Valle Alegre	n.d.	From 2009 to 2010	0.156 ± 0.027	16.3 ± 20.4%			Surface soil (0-5cm) - ²⁴⁰ Pu/ ²³⁹ Pu = Average ± 1σ (n=3)
Chile	-42.51	-72.47	Santa Barbara	n.d.	2009	0.144 ± 0.007	25.0 ± 7.6%			Surface soil (0-5cm)- Measurement ± 1σ
Chile	-20	-70	Iquique	Sea level	From 2007 to 2009	0.166 ± 0.008	9.1 ± 8.7%	AMS	Chamizo et al., 2011	Surface soil (0-5cm) - ²⁴⁰ Pu/ ²³⁹ Pu = Average ± 1σ (n=3)
Chile	-23	-70	Antofagasta	Sea level		0.12 ± 0.04	42.3 ± 29.3%			Surface soil (0-5cm) - ²⁴⁰ Pu/ ²³⁹ Pu = Average ± 1σ (n=3)
Chile	-32	-71	Punchuncavi	Sea level		0.13 ± 0.02	35.1 ± 15.4%			Surface soil (0-5cm) - ²⁴⁰ Pu/ ²³⁹ Pu = Average ± 1σ (n=3)
Chile	-33	-70	La Parva	2800		0.041 ± 0.003	99.3 ± 7.5%			Surface soil (0-5cm) - ²⁴⁰ Pu/ ²³⁹ Pu = Average ± 1σ (n=3)
Chile	-36	-71	Chillan	Sea level		0.111 ± 0.008	48.8 ± 7.7%			Surface soil (0-5cm) - ²⁴⁰ Pu/ ²³⁹ Pu = Average ± 1σ (n=3)
Chile	-42	-72	Santa Barbara	Sea level		0.134 ± 0.007	32.2 ± 7.4%			Surface soil (0-5cm) - ²⁴⁰ Pu/ ²³⁹ Pu = Average ± 1σ (n=3)
Chile	-42	-72	Chaiten	1280		0.176 ± 0.015	1.9 ± 12.9%			Surface soil (0-5cm)- Measurement ± 1σ

708
709
710
711

Table 2. $^{210}\text{Pb}_{\text{xs}}$ data, CF:CS derived ages and Temporal evolution of $^{240}\text{Pu}/^{239}\text{Pu}$ atom ratios for the Lake Chungara and Rincón del Bonete reservoir sediment cores. ^aAnalytical measurement uncertainty (k=2). ^bFor Chungara lake, ^{137}Cs analyses were not carried out for samples which have been grouped. ^cFor Chungara, ^{137}Cs activities are expressed from the time of collection (2014).

Sediment core	Samples	$^{240}\text{Pu}/^{239}\text{Pu}$	$^{239+240}\text{Pu}$ concentration (fg g ⁻¹) ^a	Proportion of Plutonium from French fallout	Depth Interval (cm)	^{137}Cs (Bq kg ⁻¹ , 2020) ^{abc}	Calendar Age (year) - CF:CS			
							Age	Minimum Age	Maximum Age	
Lake Chungara	CG 1-5	0.127 ± 0.013	31.5 ± 1.9	37.3 ± 10.7%	0.25	1.9 ± 0.2	2011	2011	2011	
					0.75	2.1 ± 0.6	2006	2006	2006	
					1.25	2.1 ± 0.6	2001	2001	2000	
					1.75	3.7 ± 0.8	1996	1996	1995	
					2.25	4.2 ± 0.4	1990	1991	1990	
	CG 6-11	0.156 ± 0.009	214.9 ± 7.3	16.3 ± 8.9%	2.75	4.4 ± 0.5	1985	1986	1984	
					3.25	7.4 ± 1.1	1980	1981	1979	
					3.75	6.0 ± 0.5	1974	1976	1973	
					4.25	7.0 ± 0.6	1969	1970	1968	
					4.75	6.0 ± 0.5	1964	1965	1962	
	CG 12-20	0.252 ± 0.015	39.8 ± 1.5	n.d.	5.25	5.6 ± 0.4	1959	1960	1957	
					5.75	2.9 ± 0.3	1953	1955	1951	
					6.25	2.5 ± 0.6	1948	1950	1946	
					7.25	1.6 ± 0.2	1938	1940	1935	
					8.25	1.4 ± 0.1	1927	1929	1924	
	Rincon del Bonete Reservoir	BON1	0.082 ± 0.005	65.3 ± 1.6	69.7 ± 6.5%	3	2.0 ± 0.7	2017	2016	2017
		BON2	0.107 ± 0.005	46.9 ± 1.3	51.7 ± 6.2%	6	1.4 ± 0.7	2014	2013	2015
		BON3	0.094 ± 0.005	54.7 ± 1.3	61.1 ± 6.3%	9	3.3 ± 0.7	2011	2010	2012
BON4		0.088 ± 0.004	53.8 ± 1.2	65.4 ± 6.0%	12	2.7 ± 0.5	2009	2007	2010	
BON5		0.087 ± 0.004	59.0 ± 1.8	66.1 ± 6.1%	15	4.1 ± 0.7	2006	2004	2008	
BON6		0.100 ± 0.005	51.4 ± 1.7	56.7 ± 6.3%	18	2.9 ± 0.7	2003	2001	2005	
BON7		0.092 ± 0.004	54.9 ± 1.7	62.5 ± 6.0%	21	1.9 ± 0.7	2000	1998	2003	
BON8		0.093 ± 0.004	54.4 ± 1.7	61.8 ± 6.0%	24	3.1 ± 1.0	1998	1995	2000	
BON9		0.082 ± 0.009	84.4 ± 6.4	69.7 ± 8.5%	27	2.9 ± 0.7	1995	1992	1998	
BON10		0.099 ± 0.006	73.7 ± 2.9	57.5 ± 6.7%	31	2.9 ± 0.4	1991	1988	1995	
Average Bonete	0.0924 ± 0.015			62.2 ± 12.2%						

712